Supplement of Biogeosciences, 23, 3887–3905, 2026
https://doi.org/10.5194/bg-23-3887-2026-supplement
© Author(s) 2026. CC BY 4.0 License.

Biogeosciences Open Access EGU

Supplement of

Denitrification as the dominant process in nitrous oxide production in the water column of two eutrophic reservoirs

Elizabeth Leon-Palmero et al.

Correspondence to: Elizabeth Leon-Palmero (el23@princeton.edu)

The copyright of individual parts of the supplement might differ from the article licence.

S1 Extended Methods: DNA extraction, PCR and qPCR assays

Water samples were pre-filtered through 3.0 µm pore-size filters prior to DNA extraction, which followed the procedure developed by Boström et al. (2004). This DNA extraction protocol combined a cell recovery step by centrifugation of 12–20 mL of the pre-filtered water, a cell lysis step with enzyme treatment (lysozyme and proteinase K), and, finally, the DNA recovery step with a co-precipitant (yeast tRNA) to improve the precipitation of low-concentration DNA. Extracted DNA served as the template for PCR and qPCR analyses to test the presence and abundance of the functional genes, respectively. For PCR analysis, we used recombinant Taq DNA Polymerase (Thermo Fisher Scientific) using the Mastercycler X50 thermal cycler (Eppendorf). Amplification was verified by using 1.5 % (w/v) agarose gel electrophoresis. qPCR plates were analyzed using SYBR Green as the reporter dye (PowerUp™ SYBR™ Green Master Mix, Thermo Fisher Scientific) in the Applied Biosystems 7500 Real-Time PCR System and the 7500 Software. Both PCR and qPCR used the standard reaction mix recipes, thermocycling conditions, and primer requirements specified by the manufacturer. Specific primers were selected from studies performed in natural freshwater samples (detailed below). DNA from pure cultures was used as positive controls and for qPCR standard preparation.

During the qPCR assays, we built a standard curve for the absolute quantification of the gene copies in the environmental samples. DNA from water column samples (3 µL) was analyzed in triplicate, together with triplicates of the no-template control, a no-primer control, and four standards also in triplicate. Automatic analysis settings were used to determine the threshold cycle (C_T) values. Dissociation curves and the melting temperature of the qPCR products were visualized to evaluate the purity of the products. Before qPCR analysis, we quantified the environmental DNA and the standards using a DNA quantitation kit (Sigma-Aldrich) based on the fluorescent dye bisBenzimide (Hoechst 33258). In each plate assay, we calculated a standard curve between the gene copy number of the standards and the C_T obtained during the qPCR run. Gene copy number in the standards was calculated from the following equation S1:

$$\text{Copy number} = \frac{\text{DNA in the reaction x } 6.022 \text{ x } 10^{23}}{\text{Length of the amplicon x } 650 \text{ x } 10^{9}} \qquad \text{(Eq. S1)}$$

where the quantity of DNA in the reaction (ng) is obtained from the sample DNA concentration (ng μL^{-1}) multiplied by the volume used in the qPCR reaction (µL). $6.022\ 10^{23}$ is the Avogadro's constant (molecules mol^{-1}), 650 is the average mass of one base pair of DNA (g mol^{-1} per bp), and 10^9 is a conversion factor. Note that the length of the amplicon (bp) is different for each gene and pair of primers. We used the standard curve to calculate the copy number of each sample using the C_T obtained during the qPCR run. Copy number was normalized to volume of water (copy number mL^{-1}), assuming 100 % recovery, as follows:

$$\text{Copy number per volume} = \frac{\text{copy number x DNA extracted}}{\text{DNA in the reaction x volume of water}} \quad \text{(Eq. S2)}$$

where the quantity of DNA extracted, and the DNA in the reaction are measured in nanograms (ng). The volume of water (mL) is the water centrifuged during the cell recovery step of the DNA extraction.

We targeted the first and rate-limiting step of the nitrification (Kowalchuk and Stephen, 2001) using the *amoA* gene, which encodes the catalytic subunit of ammonia monooxygenase. Only AOA (archaeal *amoA*) were assayed because we demonstrated in a previous study (León-Palmero et al., 2023) that AOA dominated over AOB at these reservoirs. We used the primers from Francis et al. (2005) at a final concentration of 0.4 µmol L^{-1} with an annealing temperature of 53 ºC (amplicon length 635 bp). A pure culture of *Nitrososphaera viennensis* (Stieglmeier et al., 2014) (strain EN76^T) was used for standard preparation. Comammox *amoA* genes were targeted using two degenerate PCR primer pairs, comaA-244F and comaA-659R for clade A and comaB-244F and comaB-659R for clade B of comammox bacteria (Pjevac et al., 2017) pairs with an annealing temperature was 52 ºC (amplicon length 415 bp). No positive control could be used for comammox *amoA* genes.

nirS and the *nosZ* genes were used to estimate denitrifier abundance. The *nirS* gene encodes the nitrite reductase that catalyzes the transformation of nitrite to NO during denitrification. The primers of Braker et al. (1998) nirS-1F and nirS-3R were used at a final concentration of 2 µmol L^{-1} (amplicon length 260 bp) with an annealing temperature of 62 ºC. Pure culture of *Escherichia coli* transformed with a constructed plasmid containing the *nirS* gene fragment was used for the standard preparation. The *nosZ* gene encodes the enzyme nitrous oxide reductase, responsible for the reduction of N_2O to N_2. The primers nosZ1F and nosZ1R (Henry et al., 2006) were used at a final concentration of 2 µmol L^{-1} (amplicon length was 259 bp) at an annealing temperature of 63 ºC. A pure culture of *Paracoccus denitrificans* (Beijerinck and Minkman 1910) Davis 1969 (ATCC 17741) served as a positive control for the standard quantification.

S2 Extended Methods: Scaling up to the reservoir level

The following calculations rely on several assumptions. First, we assume that the July and September profiles are representative of the entire reservoir water column during the stratification period and that depth-weighted concentrations capture vertical variability. Second, we use average reservoir volume to approximate water outflow, without accounting for short-term fluctuations in hydraulic retention time or drawdown dynamics. Third, we assume minimal nitrogen inputs from the watershed during the study period, since summer is the dry period and observed reservoir drawdown (and thus minimal inputs from streams, rain or runoff), but cannot exclude minor contributions from groundwater or episodic events. Finally, these estimates reflect net changes over the sampling interval (July–September) and should not be interpreted as annual

rates. Spatial heterogeneity and biological processes such as algal assimilation and sedimentation may also influence apparent DIN loss. Therefore, these values represent potential nitrogen removal only during the stratified season, not whole-year budgets.

We calculated the total DIN loss (mol-N) in each reservoir from July to September, following equation S3:

$$\text{Total DIN loss} = (DIN_{July} - DIN_{Sept}) \times \text{average reservoir volume} \quad \text{(Eq S3)}$$

Where DIN_{July} and DIN_{Sept} represent the mean DIN concentration (mol-N L^{-1}) in the water column of each reservoir in July and in September, respectively. Reservoir volume (L) is the average between the volume in July and September. We obtained the change in DIN concentration (%), DIN loss per day (kg-N d^{-1}) and DIN loss per surface (g-N d^{-1} m^{-2}) DIN loss percentage (%), following the equations (S4-S6):

$$\text{Change in DIN concentration (\%)} = \frac{DIN_{July} - DIN_{Sept}}{DIN_{July}} \times 100 \quad \text{(Eq. S4)}$$

$$\text{DIN loss per day} = \frac{\text{Total DIN loss} \times 14.0067 \times 10^{-3}}{\text{time}} \quad \text{(Eq. S5)}$$

$$\text{DIN loss per surface} = \frac{\text{Total DIN loss} \times 14.0067}{\text{time} \times \text{reservoir area}} \quad \text{(Eq. S6)}$$

Where 14.0067 is the molar mass of nitrogen (g mol-N^{-1}), and 10^{-3} is the factor to convert grams to kilograms. Time is the number of days between the sampling in July and the sampling in September, and the reservoir area is measured in m^2. Similarly, we also calculated the mean N_2O production per day (kg-N d^{-1}), and the mean N_2O prod. per surface (g-N d^{-1} m^{-2}) following equations (S7 and S8):

$$\text{Mean } N_2O \text{ prod. per day} = \text{Mean } N_2O \text{ prod.} \times 14.0067 \times 10^{-12} \times \text{reservoir volume} \quad \text{(Eq. S7)}$$

$$\text{Mean } N_2O \text{ prod. per surface} = \frac{\text{Mean } N_2O \text{ prod. per day} \times 10^{3}}{\text{reservoir area}} \quad \text{(Eq. S8)}$$

where the mean N_2O prod. (nmol-N L^{-1} d^{-1}) is the mean for the total N_2O production in the water column for each reservoir. This total N_2O production was obtained as the sum of the production of N_2O from ammonium and from NO_3^- at each layer. 10^{-12} (to convert nmol to mol and g to kg) and 10^3 (to convert kg to g) are conversion factors. The reservoir volume (L) is the average between the volume in July and the volume in September, and the time is the number of days between the sampling in July and the sampling in September. Finally, we calculated the N_2O production per DIN loss (%) from the DIN loss per day (kg-N d^{-1}) and the mean N_2O production per day (kg-N d^{-1}) as follows (Eq. S9):

$$N_2O \text{ prod. per DIN loss} = \frac{\text{Mean total } N_2O \text{ prod. per day}}{\text{DIN loss per day}} \times 100 \quad \text{(Eq. S9)}$$

Table S1. Dissolved N_2O concentration (µmol-N L^{-1}), and saturation (%), dissolved organic carbon (DOC) concentration (µmol-C L^{-1}), nitrate (NO_3^-), nitrite (NO_2^-), and ammonium (NH_4^+) concentrations (µmol-N L^{-1}), and chlorophyll *a* (Chl *a*) concentration (µg L^{-1}) measured during the July and September sampling in Cubillas and Iznájar reservoirs. SE = standard error. SD = standard deviation.

Reservoir	ID	Depth	Dissolved N_2O (Mean ± SE)	N_2O saturation (Mean ± SE)	DOC (Mean ± SD)	NO_3^-	NO_2^-	NH_4^+	Chl *a*
Cubillas (July)	#1	Epilimnion (2 m)	0.11 ± 0.00	739 ± 27	247.7 ± 4.6	376.0	13.8	1.6	5.4
	#2	Oxycline (7 m)	0.71 ± 0.01	4075 ± 29	227.4 ± 6.5	333.6	29.8	0.0	13.9
	#3	Bottom (9.5 m)	6.38 ± 0.04	31822 ± 207	246.4 ± 8.6	254.0	17.0	4.3	6.9
Cubillas (September)	#4	Epilimnion (0.5 m)	0.22 ± 0.00	1404 ± 11	246.5 ± 1.1	177.8	19.3	2.5	18.1
	#5	Epilimnion (2.5 m)	0.22 ± 0.00	1424 ± 10	235.9 ± 5.8	176.7	19.3	0.0	14.6
	#6	Bottom (6.2 m)	0.42 ± 0.00	2565 ± 27	217.6 ± 0.2	132.7	33.0	6.9	12.7
Iznájar (July)	#7	Epilimnion (3 m)	0.05 ± 0.00	357 ± 5	228.0 ± 9.5	367.6	20.6	0.0	6.3
	#8	Oxycline (8 m)	0.18 ± 0.00	1059 ± 10	191.0 ± 0.5	361.6	38.1	5.7	12.4
	#9	Hypolimnion (20 m)	0.26 ± 0.00	1137 ± 7	198.5 ± 0.6	391.8	9.6	0.0	4.7
Iznájar (September)	#10	Epilimnion (5 m)	0.20 ± 0.00	1308 ± 17	217.3 ± 3.0	335.3	22.9	0.0	7.0
	#11	Oxycline (11 m)	0.47 ± 0.00	3072 ± 8	192.1 ± 2.8	314.6	40.8	0.0	8.3
	#12	Hypolimnion (23 m)	3.60 ± 0.00	16585 ± 105	186.0 ± 8.3	338.0	2.8	8.7	3.8

Table S2. Concentrations (µmol-N L^{-1}) and isotopic composition (‰) of the nitrate ($\delta^{15}N\text{-}NO_3^-$), the nitrite ($\delta^{15}N\text{-}NO_2^-$), and the N_2O pools ($\delta^{15}N\text{-}N_2O$ and $\delta^{18}O\text{-}N_2O$) in July and September in Cubillas and Iznájar reservoir. n.d. = not determined. All $\delta^{15}N$ values are reported relative to Air-N_2, and all $\delta^{18}O$ values are reported relative to VSMOW.

Reservoir	ID	Depth	$\delta^{15}N\text{-}N_2O$	$\delta^{18}O\text{-}N_2O$	NO_3^-	$\delta^{15}N\text{-}NO_3^-$	NO_2^-	$\delta^{15}N\text{-}NO_2^-$
Cubillas (July)	#1	Epilimnion (2 m)	2.7 ± 1.8	57.6 ± 0.2	376.0	11.9 ± 0.3	13.8	-36.8 ± 0.3
	#2	Oxycline (7 m)	-1.5 ± 0.0	55.5 ± 0.5	333.6	11.3 ± 0.2	29.8	-6.9 ± 0.1
	#3	Bottom (9.5 m)	-2.1 ± 0.1	41.6 ± 0.2	254.0	11.0 ± 0.2	17.0	10.9 ± 0.1
Cubillas (September)	#4	Epilimnion (0.5 m)	3.5 ± 0.0	57.2 ± 0.1	177.8	13.4 ± 0.3	19.3	-11.7± 0.7
	#5	Epilimnion (2.5 m)	3.6 ± 0.0	57.3 ± 0.1	176.7	11.6 ± 0.2	19.3	-11.9 ± 0.1
	#6	Bottom (6.2 m)	1.5 ± n.d.	64.4 ± n.d.	132.7	11.8 ± n.d.	33.0	-0.6 ± n.d.
Iznájar (July)	#7	Epilimnion (3 m)	-4.2 ± 0.8	48.8 ± 0.5	367.6	10.1 ± 0.0	20.6	-26.8 ± 0.1
	#8	Oxycline (8 m)	-7.4 ± 2.5	49.0 ± 0.7	361.6	10.4 ± 0.2	38.1	-13.3± 0.0
	#9	Hypolimnion (20 m)	-8.7 ± 3.7	51.8 ± 3.5	391.8	8.9 ± 0.1	9.6	-18.6 ± 0.2
Iznájar (September)	#10	Epilimnion (5 m)	-7.5 ± 0.1	49.4 ± 0.1	335.3	12.6 ± 2.8	22.9	-21.4 ± 0.0
	#11	Oxycline (11 m)	-7.2 ± 0.1	48.7 ± 0.3	314.6	9.7 ± 0.1	40.8	-9.1 ± 0.0
	#12	Hypolimnion (23 m)	-2.3 ± 0.0	52.5 ± 0.1	338.0	11.8 ± 1.3	2.8	8.8 ± 0.1

Table S3. Summary of the production rates measured during the incubations with $^{15}N\text{-}NH_4^+$ and $^{15}N\text{-}NO_3^-$. NO_2^- or N_2O turnover was the proportion between concentration and production. NP = not performed.

Reservoir	Depth	N_2O production from NH_4^+	Ammonia oxidation	Nitrification	N_2O yield from nitrification	N_2O production from NO_3^-	Nitrate reduction to nitrite	NO_2^- turnover	N_2O yield from denitrification	Total N_2O production	N_2O turnover
		nmol-N L^{-1} d^{-1}	nmol-N L^{-1} d^{-1}	µmol-N L^{-1} d^{-1}	%	nmol-N L^{-1} d^{-1}	µmol-N L^{-1} d^{-1}	d	%	nmol-N L^{-1} d^{-1}	d
Cubillas (July)	Epilimnion (2 m) #1	2.08 ± 0.15	0.0	26.9 ± 5.0	0.008	NP	NP	NP	NP	2.1	53
	Oxycline (7 m) #2	0.15 ± 0.06	0.0	13.3 ± 1.1	0.001	15.5 ± 5.7	33.2 ± 1.3	0.9	0.047	15.7	45
	Bottom (9.5 m) #3	48.57 ± 8.35	0.0	56.1 ± 18.6	0.086	0.2 ± 0.0	30.8 ± 2.5	0.6	0.001	48.7	131
Cubillas (September)	Epilimnion 1 (0.5 m) #4	0.47 ± 0.20	0.0	15.6 ± 3.4	0.003	NP	NP	NP	NP	0.5	468
	Epilimnion 2 (2.5 m) #5	0.06 ± 0.00	0.0	6.1 ± 1.5	0.001	NP	NP	NP	NP	0.1	3669
	Bottom (6.2 m) #6	0.21 ± 0.03	0.0	15.4 ± 5.4	0.001	18.1 ± 3.1	13.7 ± 1.2	2.4	0.132	18.3	23
Iznájar (July)	Epilimnion (3 m) #7	0.83 ± 0.00	0.0	5.4 ± 1.4	0.015	NP	NP	NP	NP	0.8	63
	Oxycline (8 m) #8	3.72 ± 0.72	0.0	36.7 ± 14.8	0.010	10.0 ± 0.8	28.6 ± 0.4	1.3	0.035	13.8	13
	Hypolimnion (20 m) #9	0.02 ± 0.00	0.0	9.0 ± 6.0	0.000	4.8 ± 0.5	17.4 ± 0.1	0.6	0.027	4.8	54
Iznájar (September)	Epilimnion (5 m) #10	0.93 ± 0.25	0.0	2.9 ± 1.0	0.033	NP	NP	NP	NP	0.9	211
	Oxycline (11 m) #11	0.59 ± 0.06	0.0	3.7 ± 1.2	0.016	61.0 ± 38.9	10.1 ± 1.5	4.1	0.603	61.6	8
	Hypolimnion (23 m) #12	0.09 ± 0.04	215.8 ± 38.0	0.0	-	0.4 ± 0.1	12.9 ± 0.5	0.2	0.003	0.4	8197

Table S4. In situ abundance of the archaeal *amoA* (mean ± SD, copies mL^{-1}), *nirS* (mean ± SD, copies mL^{-1}), and *nosZ* (mean ± SD, copies mL^{-1}) genes detected in July and September in Cubillas and Iznájar reservoirs. SD = standard deviation. NP = not performed.

Reservoir	ID	Depth	Archaeal *amoA* (copies mL^{-1})	*nirS* (copies mL^{-1})	*nosZ* (copies mL^{-1})
Cubillas (July)	#1	Epilimnion (2 m)	0	$5.9 \times 10^4 \pm 5.5\ 10^3$	NP
	#2	Oxycline (7 m)	$2.7 \times 10^3 \pm 385$	$5.3 \times 10^4 \pm 2.3\ 10^4$	NP
	#3	Bottom (9.5 m)	0	$5.3 \times 10^5 \pm 3.6\ 10^5$	800 ± 54
Cubillas (September)	#4	Epilimnion (0.5 m)	$1.1 \times 10^3 \pm 214$	$4.5 \times 10^4 \pm 2.7\ 10^4$	NP
	#5	Epilimnion (2.5 m)	609 ± 120	$5.6 \times 10^4 \pm 1.3\ 10^4$	NP
	#6	Bottom (6.2 m)	324 ± 285	$2.8 \times 10^5 \pm 3.2\ 10^3$	913 ± 68
Iznájar (July)	#7	Epilimnion (3 m)	$1.3 \times 10^3 \pm 120$	$8.1 \times 10^4 \pm 2.6\ 10^4$	NP
	#8	Oxycline (8 m)	995 ± 441	$4.6 \times 10^5 \pm 6.1\ 10^4$	NP
	#9	Hypolimnion (20 m)	$1.3 \times 10^3 \pm 110$	$4.8 \times 10^5 \pm 4.6\ 10^5$	$1.2 \times 10^3 \pm 302$
Iznájar (September)	#10	Epilimnion (5 m)	$1.1 \times 10^3 \pm 216$	$1.7 \times 10^5 \pm 3.6\ 10^4$	NP
	#11	Oxycline (11 m)	$1.6 \times 10^3 \pm 24$	$8.0 \times 10^5 \pm 2.3\ 10^5$	NP
	#12	Hypolimnion (23 m)	$1.1 \times 10^3 \pm 406$	$4.7 \times 10^6 \pm 1.3\ 10^6$	$2.1\ 10^3 \pm 198$

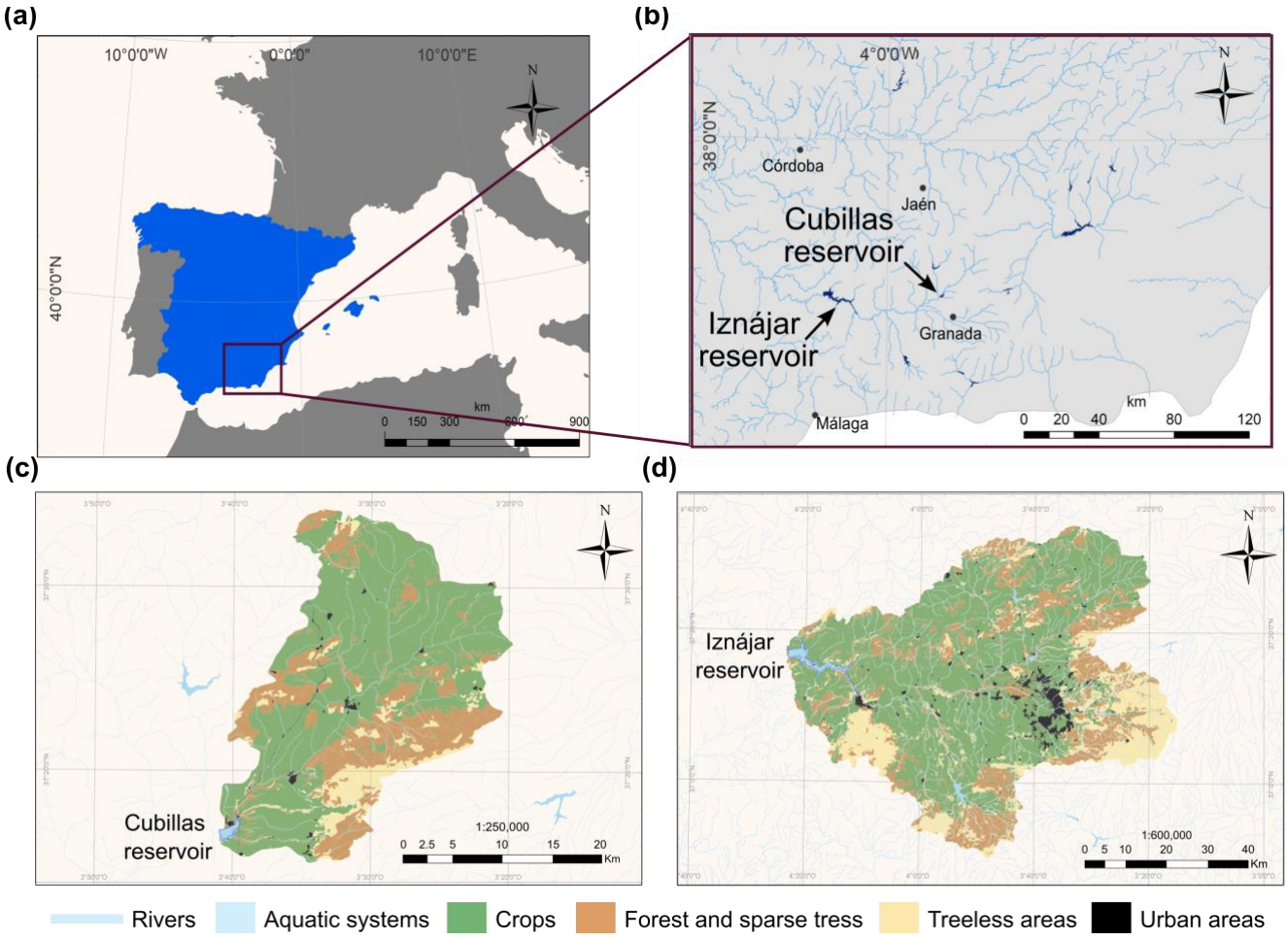

Figure S1. Study sites. (a) The square delimited the region in the Iberian Peninsula where the reservoirs are located; (b) study reservoirs. Land use in the watershed of Cubillas reservoir (c), and Iznájar reservoir (d). Note the different scales in the maps. Detailed maps and information on the watersheds and land uses in these reservoirs can be found in León-Palmero et al. (2020).

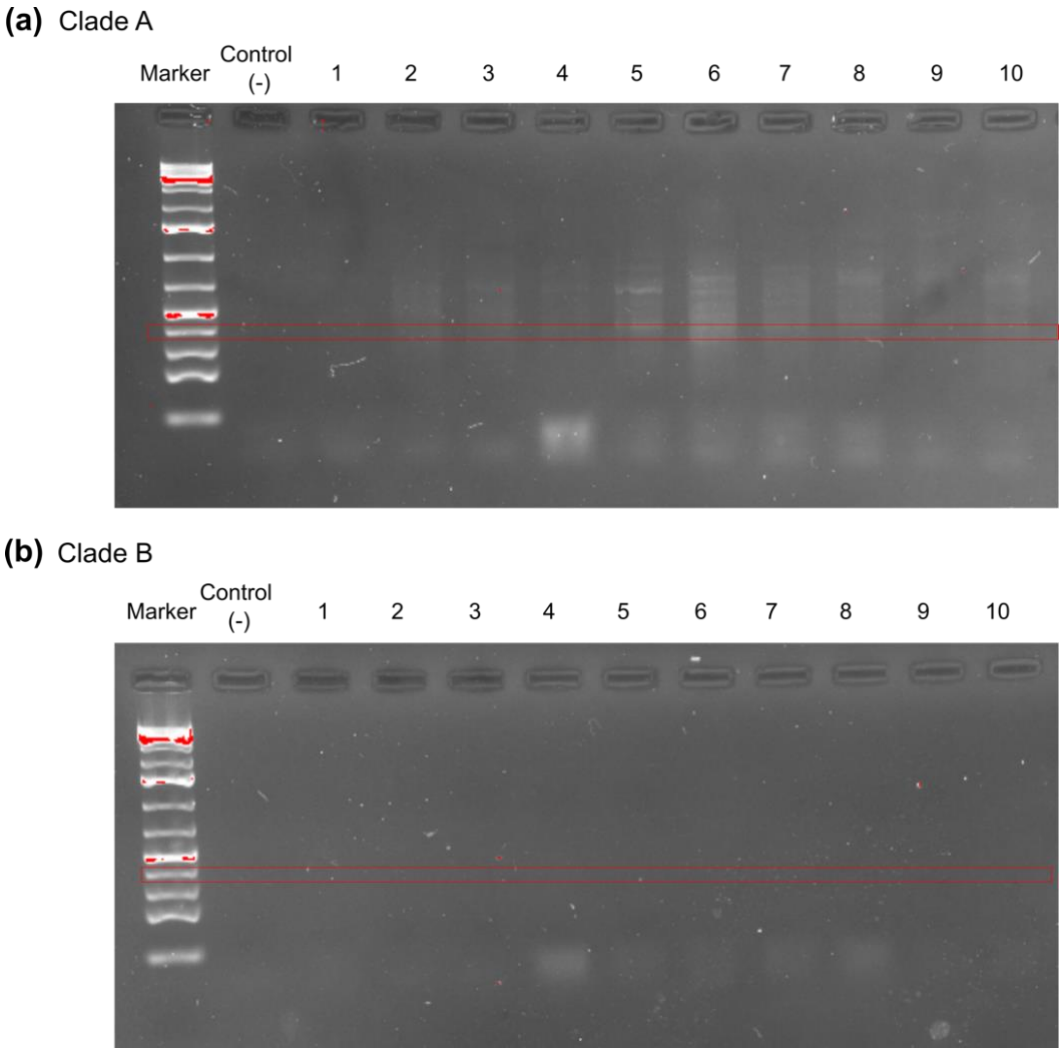

Figure S2. Results of the PCR for the comammox *amoA* genes. PCR results resolved on 1.5 % agarose gel electrophoresis. We used the two degenerate PCR primer pars (Pjevac et al., 2017) to target the clade A (a) or the clade B (b) of comammox bacteria, with an expected amplicon length of 415 bp. The red boxes stand for the ≈ 400 bp bands. In this order: the DNA marker, the negative controls, and samples (1-10). The samples displayed correspond to the following depths: 1: Cubillas epilimnion in July (2 m); 2: Iznájar epilimnion in July (3 m); 3: Iznájar oxycline in July (8 m); 4: Iznájar hypolimnion in July (20); 5: Cubillas epilimnion in September (0.5 m); 6: Cubillas epilimnion in September (2.5 m); 7: Cubillas oxycline-bottom in September (6.2 m); 8: Iznájar epilimnion in September (5 m); 9: Iznájar oxycline in September (11 m); and 10: Iznájar hypolimnion in September (23 m). We provide more details in the Methods section.

References

Boström, K. H., Simu, K., Hagström, Å., and Riemann, L.: Optimization of DNA extraction for quantitative marine bacterioplankton community analysis, Limnol. Oceanogr. Methods, 2, 365–373, https://doi.org/10.4319/lom.2004.2.365, 2004.

Braker, G., Fesefeldt, A., and Witzel, K.-P.: Development of PCR primer systems for amplification of nitrite reductase genes (*nirK* and *nirS*) to detect denitrifying bacteria in environmental samples, Appl. Environ. Microbiol., 64, 3769–3775, https://doi.org/10.1128/AEM.64.10.3769-3775.1998, 1998.

Francis, C. A., Roberts, K. J., Beman, J. M., Santoro, A. E., and Oakley, B. B.: Ubiquity and diversity of ammonia-oxidizing archaea in water columns and sediments of the ocean, PNAS, 102, 14683–14688, https://doi.org/10.1073/pnas.0506625102, 2005.

Henry, S., Bru, D., Stres, B., Hallet, S., and Philippot, L.: Quantitative detection of the *nosZ* gene, encoding nitrous oxide reductase, and comparison of the abundances of 16S rRNA, *narG*, *nirK*, and *nosZ* genes in soils, Appl. Environ. Microbiol., 72, 5181–5189, https://doi.org/10.1128/AEM.00231-06, 2006.

Kowalchuk, G. A. and Stephen, J. R.: Ammonia-oxidizing bacteria: A model for molecular microbial ecology, Annu. Rev. Microbiol., 55, 485–529, https://doi.org/10.1146/annurev.micro.55.1.485, 2001.

León-Palmero, E., Morales-Baquero, R., and Reche, I.: Greenhouse gas fluxes from reservoirs determined by watershed lithology, morphometry, and anthropogenic pressure, Environ. Res. Lett., 15, 044012, https://doi.org/10.1088/1748-9326/ab7467, 2020.

León-Palmero, E., Morales-Baquero, R., and Reche, I.: P inputs determine denitrifier abundance explaining dissolved nitrous oxide in reservoirs, Limnology and Oceanography, 68, 1734–1749, https://doi.org/10.1002/lno.12381, 2023.

Pjevac, P., Schauberger, C., Poghosyan, L., Herbold, C. W., van Kessel, M. A. H. J., Daebeler, A., Steinberger, M., Jetten, M. S. M., Lücker, S., Wagner, M., and Daims, H.: *amoA*-targeted polymerase chain reaction primers for the specific detection and quantification of comammox *Nitrospira* in the Environment, Front. Microbiol., 8, https://doi.org/10.3389/fmicb.2017.01508, 2017.

Stieglmeier, M., Mooshammer, M., Kitzler, B., Wanek, W., Zechmeister-Boltenstern, S., Richter, A., and Schleper, C.: Aerobic nitrous oxide production through N-nitrosating hybrid formation in ammonia-oxidizing archaea, ISME J, 8, 1135–1146, https://doi.org/10.1038/ismej.2013.220, 2014.